Growth of the transient planar state in cholesteric liquid crystals

Min-Hyong Lee, Young-Chol Yang, Jae-Eun Kim, and Hae Yong Park
Department of Physics, Korea Advanced Institute of Science and Technology, Kusung-dong 373-1, Yusong-gu, Daejeon 305-701, Korea
(Received 12 March 2003; published 3 November 2003)

Growth and propagation of the transient planar state in the transition of cholesteric liquid crystals from the homeotropic to the planar state was investigated by both experiments and numerical simulations for planar boundary conditions. Interference fringes observed in the measured reflection spectra during the evolution of the transient planar state have not been reported in the previous study. These interference fringes caused by a Fabry-Perot interferometric structure formed in the cell show that the transient planar state grows from the surfaces and propagates toward the bulk region in the planar sample. Our experimental results for the growth of transient planar state in planar boundary conditions are consistent with the previously reported simulation studies.

DOI: 10.1103/PhysRevE.68.051701 PACS number(s): 61.30.−v, 77.84.Nh, 78.20.Bh, 78.20.Jq

I. INTRODUCTION

Cholesteric liquid crystals have two stable states between parallel glass substrates: a planar (P) state and a focal conic (FC) state. In the P state, the helical axes of cholesteric liquid crystals are normal to the plates and this P state makes a Bragg reflection in the spectral range of $n_o P_0 \leqslant \lambda \leqslant n_e P_0$, where P_0 is the intrinsic pitch of the P state, and n_o and n_e are the ordinary and extraordinary refractive indices of the liquid crystal, respectively. When an electric or magnetic field is applied, the P state makes a transition to the FC state [1], where the helical axes are parallel to the plates and distorted in the plane of the plates. At still higher field, the helical structure of cholesteric liquid crystals becomes untwisted and the FC state makes a transition to a nematiclike homeotropic (H) state. The material in the field-induced H state relaxes either to the P state or to the FC state depending on the manner the external field is removed. When the applied field is decreased gradually, the system proceeds to the FC state, but upon a sudden removal of the field it eventually relaxes into the equilibrium P state. There have been reports suggesting that an intermediate transient planar (TP) state exists during this H to P transition of cholesteric liquid crystals [2–4]. The TP state is similar to the P state as it has an in-plane helical structure with the helical axes normal to the plates. However, this state has a longer pitch than the P state.

Many experiments and numerical simulations have been carried out [5–9] to understand the transformation process from the H to the P state. A diagram of the full H to TP to P transition in planar boundary conditions, as it is currently understood, may be seen in Fig. 1. The field induced H state makes a transition to the TP state when the external field is removed. But the TP state which occurs at the early stage of the H to P relaxation is not stable, and the system makes a transition to the equilibrium P state through the FC state [5,8]. The director structure during the transition of the H to the P state had been studied using numerical simulations [6,8,9]. Simulation studies of Anderson *et al.* show that the propagation process of the TP state with planar boundary conditions is different from that with homeotropic boundary conditions [8]. According to their report, the TP state grows in from the surfaces of the cell and propagates to the bulk for planar boundary conditions. This may be due to the higher energy at the surfaces than in the bulk. Their simulation results also show that with homeotropic boundary conditions the TP state grows from the bulk and propagates to the surfaces. In the case of the homeotropic boundary conditions there are no distortions of the directors near the surfaces. Therefore, the thermal fluctuations of the directors in the bulk may become the source of the transition causing the transition to begin from the bulk. These results for the growth and propagation of the TP state for the planar and homeotropic boundary conditions were numerically simulated and, to our knowledge, have not been confirmed experimentally yet.

In this study, we experimentally investigate the evolution of the TP state during the H to P transition for planar boundary conditions. With reflection spectra measured and some numerical simulations for the initial relaxation of the system, we explain, for planar boundary conditions, where the TP state begins and propagates to.

II. EXPERIMENTAL PROCEDURES

A. Experiment

As shown in Fig. 2, our experimental system consists of a light source block, an optical component block, and an electrical component block. The light source block includes a high power Xe lamp and a monochromator. Reflection spectra are measured by a photomultiplier tube (Hamamatsu R-405). The electric component block includes a digital oscilloscope (Hewlett Packard 54501A), a function generator (Tektronix FG5010), and a voltage amplifier (Krohn-Hite 7500). A nearly parallel beam of monochromatic light was incident on the sample and the reflectance was measured employing two cross polarizers to prevent the light reflected from the glass of the LC cell from coming into the photomultiplier tube. The wavelength was scanned from 410 to 680 nm with an interval of 0.5 nm and time was scanned with an interval of 0.02 ms. The voltage applied to the sample was a 1 kHz, 150 V_{pp} square wave. The cell temperature was kept constant throughout the measurement.

The planar boundary conditions were achieved by spin coating a planar SE 5291 polyimide (Nissan Chemical Ind.,

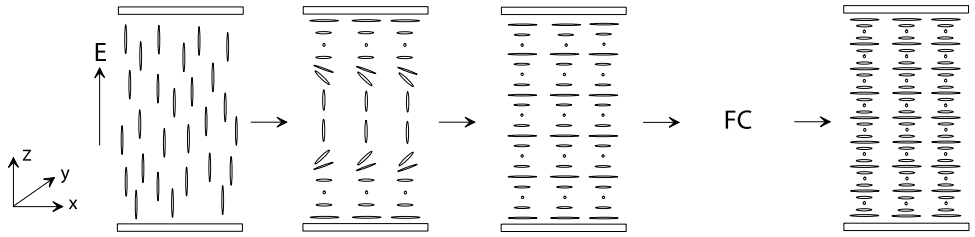

FIG. 1. Diagram of the homeotropic-planar transition for planar boundary conditions as currently understood.

Ltd.) which was then rubbed with a felt cloth. The pretilt angle of this sample, which was measured after filling the nematic liquid crystals (Merck ZLI 2293) using the crystal rotation method [10], was $(6.1\pm0.5)°$.

The cholesteric liquid crystals used in this experiment were made by mixing Merck ZLI 2293 liquid crystal and ZLI 811 chiral dopants in the ratio of 2:1. The maximum reflection region of this mixture in equilibrium ranged from 434 to 468 nm with the center ($\lambda_{P,center}$) at 451 nm. The intrinsic pitch P_0 of the mixture was measured to be (290 ± 10) nm using the Grandjean-Cano method [11,12]. Therefore, from the relation between the center wavelength of the reflection peak ($\lambda_{P,center}$) and the pitch of the equilibrium P state $\lambda_{C,P}=\bar{n}P_0$ the average refractive index $\bar{n}$ is calculated to be 1.56. The dielectric constants, $\epsilon_\perp$ and $\epsilon_\parallel$ were measured in the P and H states, respectively, by connecting a capacitor of known capacitance in series with the sample, and measuring the voltage drop across it as a function of the input voltage (1 kHz sinusoidal wave). $\epsilon_\perp$ and $\epsilon_\parallel$ were measured to be 4.7 and 9.7, respectively, and thus the dielectric anisotropy $\Delta\epsilon$ is $+5.0$. The cell gap, which was measured interferometrically, was 5.2 μm. All these measured values were used for our theoretical simulation studies and are listed in Table I.

B. Numerical simulations

The free energy density of a cholesteric liquid crystal system, in terms of the director **n** is expressed as [13]:

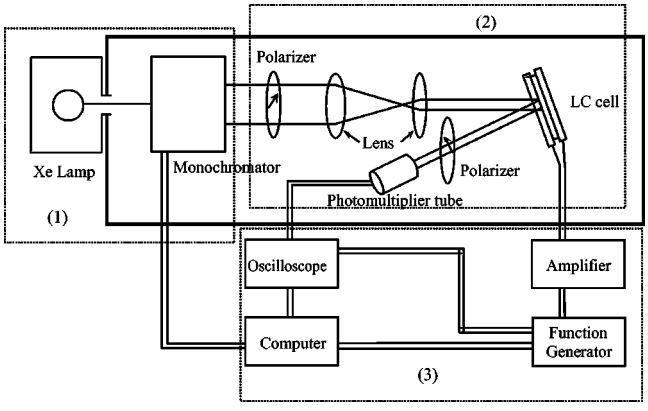

FIG. 2. Schematics of experimental arrangement.

$$f=\tfrac{1}{2}K_{11}(\nabla\cdot\hat{\mathbf{n}})^2+\tfrac{1}{2}K_{22}(\hat{\mathbf{n}}\cdot\nabla\times\hat{\mathbf{n}}+q_0)^2+\tfrac{1}{2}K_{33}(\hat{\mathbf{n}}\times\nabla\times\hat{\mathbf{n}})^2, \quad (1)$$

where K_{11}, K_{22}, and K_{33} are the elastic constants for splay, twist, and bend deformation, respectively.

The director structure of a liquid crystal system can be obtained on the basis of the fact that the system acts to minimize the free energy. Ignoring the flow of directors, the Euler-Lagrange equation to minimize Eq. (1) yields [14]

$$\gamma\frac{dn_i}{dt}=-\frac{\delta f}{\delta n_i}+\lambda n_i, \quad i\in\{x,y,z\}, \quad (2)$$

where γ is the rotational viscosity, n_i denotes the i component of director vector, and λ is a Lagrange multiplier used to maintain the unit length of the director. We used the same method that was employed in Ref. [8] to calculate the director structure numerically. The Q tensor relaxation method was used to avoid discretization error [9,15]. Flow effects and thermal fluctuations of directors were ignored. At the cell substrates, the Neuman boundary condition with Rapini-Popoular surface free energy was employed [16].

TABLE I. The parameters used in the numerical calculation of director evolution with the Q tensor relaxation method and reflection spectra with the Berreman 4×4 method.

	Symbol	Value
Pitch of the cholesteric LC	P_0	290 nm
Splay elastic constant	K_{11}	6.3 pN
Twist elastic constant	K_{22}	5.2 pN
Bend elastic constant	K_{33}	7.4 pN
Rotational viscosity	γ	90 mPa·s
Cell thickness	d	5.2 μm
Polar anchoring energy	A_p	5×10^{-4}J/m^2
Pretilt angle	α	6.1°
Refractive index of extraordinary axis	n_e	1.62
Refractive index of ordinary axis	n_o	1.52
Dielectric constant perpendicular	$\epsilon_\perp$	4.7
Dielectric constant parallel	$\epsilon_\parallel$	9.7
Light incident angle	θ	3.0°
Thickness of spatial mesh grid		d/2560
Period of temporal mesh grid		1 ns

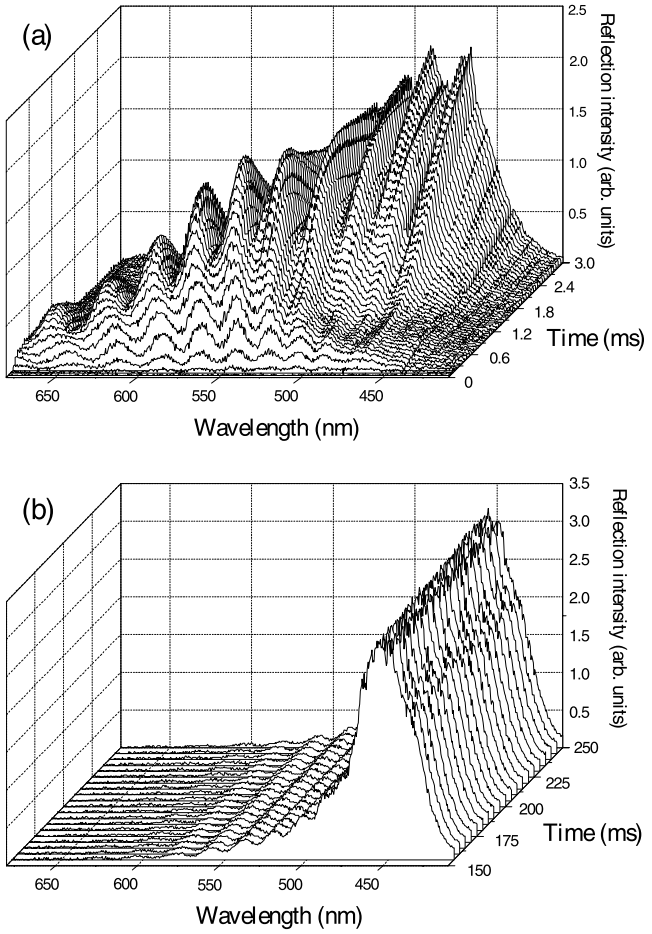

FIG. 3. Optical reflectance vs wavelength and time for the planar sample during the transition from the H state to the P state for the time (a) 0–3.0 ms and (b) 150–250 ms. (Note that the reflection band for the TP state has completely disappeared and the system is now in the P state).

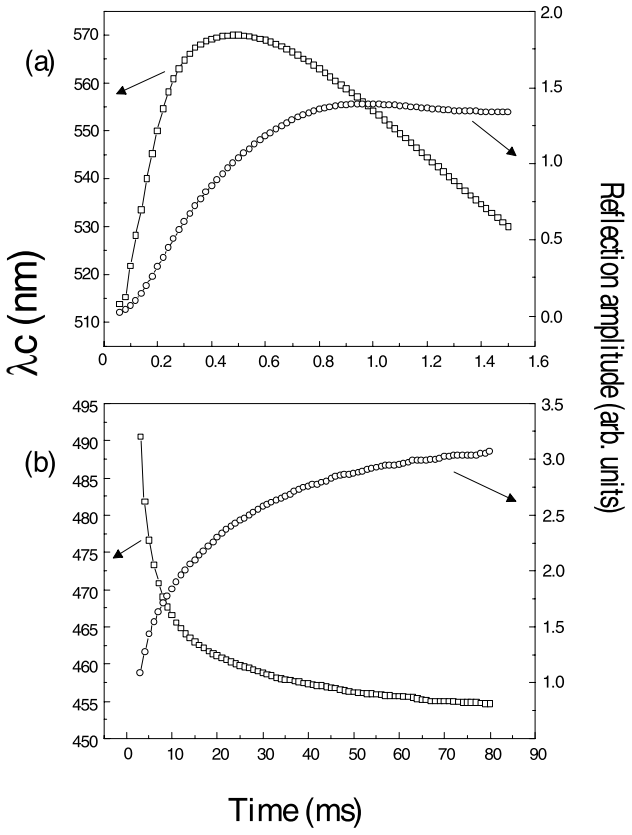

FIG. 4. Time evolution of the center wavelength of the reflection band λ_c and the reflection amplitude for the planar sample during (a) the initial H to P transition and (b) further relaxation of the system into the equilibrium P state.

The optical reflection spectra were calculated by the Berreman 4×4 method [17], which is suitable for stratified optical media and systems where reflection cannot be ignored. To avoid the truncation error of the naive Taylor expansion method, we applied the Caley-Hamilton theorem in computing the transfer matrix [18–20].

III. RESULTS AND DISCUSSION

Figure 3 shows a three-dimensional graph of reflection intensity vs wavelength and time, which was constructed from the measured reflected signals for our planar sample during the transition from the H to P state. The incident angle of monochromatic light on the LC cell was 3.0°. Figure 3(a) represents the relaxation process for the early stages of the transition and Fig. 3(b) shows the reflection spectra taken after sufficient time has lapsed so that the system has fully reached the equilibrium P texture. In Fig. 3(a), a broad reflection spectrum, which is centered at around 570 nm, corresponds to the reflection spectrum of the TP state. This TP band consists of sharp interference fringes and these fringes vanish after sufficiently long time when the TP state is completely died out and the equilibrium planar texture is formed in the cell [see Fig. 3(b)]. To our knowledge, these interference fringes observed in the reflection spectra of a cholesteric cell during the growth of the TP state have not been reported in previous studies. The TP state lasts for about 1–2 ms and then the P band starts to grow around $\lambda=510$ nm. The reflection intensity of the P spectrum increases with time with the center wavelength moving slowly to its equilibrium P wavelength 451 nm.

Figure 4 shows the time evolution of the center wavelength λ_c and the peak amplitude of (a) the TP reflection band and (b) the P reflection band for our cell. As shown in Fig. 4(a), the center wavelength λ_c starts at about 514 nm and evolves toward longer wavelengths at the early stage of the transition. However, during this time interval, the reflected intensity is quite weak, implying that the helical structure is hardly formed in the cell at this stage. As time goes on, the reflection intensity becomes stronger with the formation of the helical structure in the cell. λ_c of the TP band reaches the maximum value of 570 nm at $t=0.5$ ms, which is the reflection wavelength of the TP state for our system, and then, as shown in Fig. 4(b), slowly moves toward the equilibrium planar reflection wavelength 451 nm with the peak amplitude increasing.

Interference fringes in Fig. 3(a) are related with the growing process of the TP state. To see the propagating process of

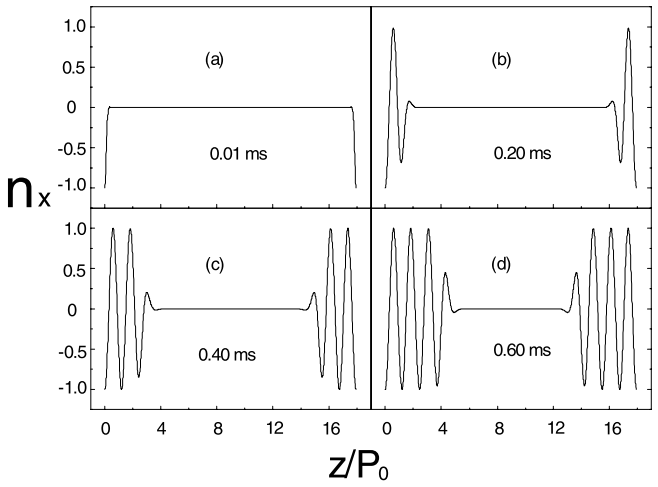

FIG. 5. Simulated time evolution of $n_x(z)$ during the initial H to P transition for the planar sample. Times are (a) 0.01 ms, (b) 0.20 ms, (c) 0.40 ms, and (d) 0.60 ms. The z axis is normal to the substrates.

the TP state, we numerically simulate the time evolution of the spatial configuration of n_x, the x component of the director, as shown in Fig. 5. As can be seen in Fig. 5(a), at the early time of the transition, the value of n_x is zero in all region of the sample except for the surfaces. Nonzero value of n_x near the surfaces is due to the planar boundary conditions at the surface. As time goes on, the directors of liquid crystals are twisted from the surfaces and the sample transforms from the nematic phase to the cholesteric state. The reason why the transition begins from the surfaces with planar boundary conditions is related to the free energy density of liquid crystals. According to the simulation results for the planar sample, the value of the director component parallel to the plane of the substrates at the surfaces is almost 1.0 the moment the transition to the TP state begins. This is because of the surface polar anchoring. This component of the director rapidly decreases to zero as the director directs away from the surfaces. As a result, the director configuration near the surfaces is highly distorted, resulting in the higher free energy density near the surfaces than in the bulk. Therefore, the system near the surfaces is unstable, originating the transition to the TP state to begin from the surfaces. As the transition to the cholesteric phase begins from two surfaces and propagates toward the center of the cell, a spatially cholesteric-nematic-cholesteric structure is formed in the cell as can be seen in Figs. 5(b)–(d). Because a cholesteric structure reflects one component of the circularly polarized light, this spatially cholesteric-nematic-cholesteric structure will serve as a Fabry-Perot interferometer. The liquid crystal material of cholesteric texture near the two surfaces plays the role of reflecting mirrors and the bulk region of nematic phase acts as a cavity resonator. Thereby, periodic interference fringes appear in the measured reflection spectra of the TP state.

Figure 6(a) displays the numerically simulated reflection spectra for our system as the TP state grows in the cell. These reflection spectra are obtained from the director configurations as shown in Fig. 5 employing the Berreman 4 $\times$4 method [17]. The interference fringes due to the Fabry-Perot interferometric structure are clearly shown in the numerically calculated spectra. Our experimentally measured spectra for the planar sample, shown in Fig. 6(b), agree well with the simulation results exhibiting such periodic interference fringes. This interference pattern in the reflection spectra will be a convincing experimental evidence that the TP state indeed starts to grow from the surfaces and propagates toward the bulk as reported mainly from theoretical simulations [8]. The experimental spectra gradually stray from the simulation results after 0.5 ms in transition. It appears that the system proceeds to the FC state before the perfect TP state, i.e., perfect helical structure in all region of the cell, is formed in the cell [5,8]. As the TP state has higher energy than that of the P state, the system in this phase is metastable and eventually reaches the equilibrium P state. In the numerical simulation, thermal fluctuations or impurities which may exist in the cell are not considered, so that the system will relax to the perfect TP state as shown in Fig. 6(a). However, in the real sample, such thermal fluctuations or impurities may exist and cause the system to transform to the FC state before the perfect TP state is fully reached. The picture, that the system will pass to the FC state before the perfect helical structure is realized in the cell, is also manifested in Fig. 4.

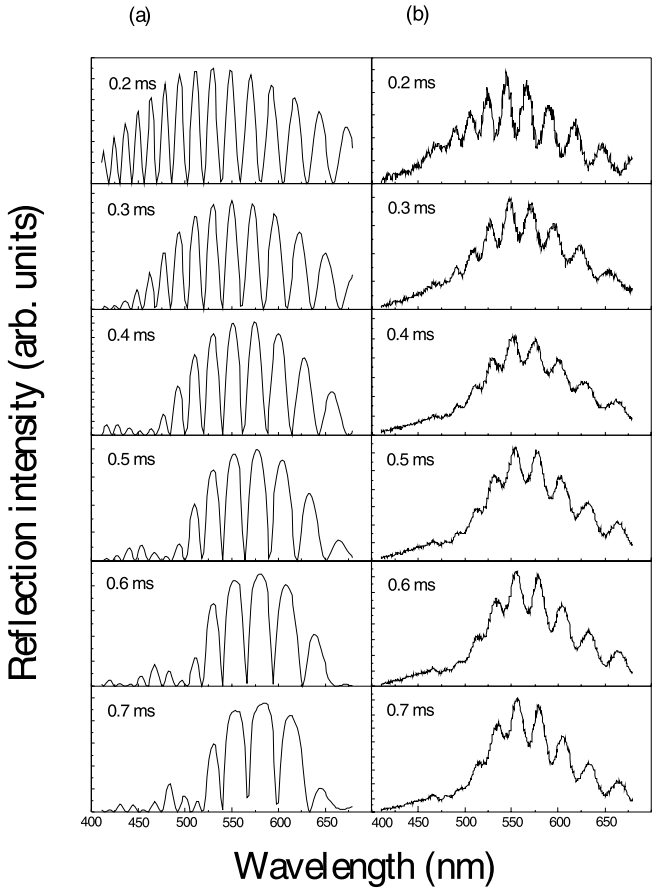

FIG. 6. (a) Numerically simulated and (b) experimentally obtained reflection spectra during the early stages of the H to P transition for planar boundary conditions.

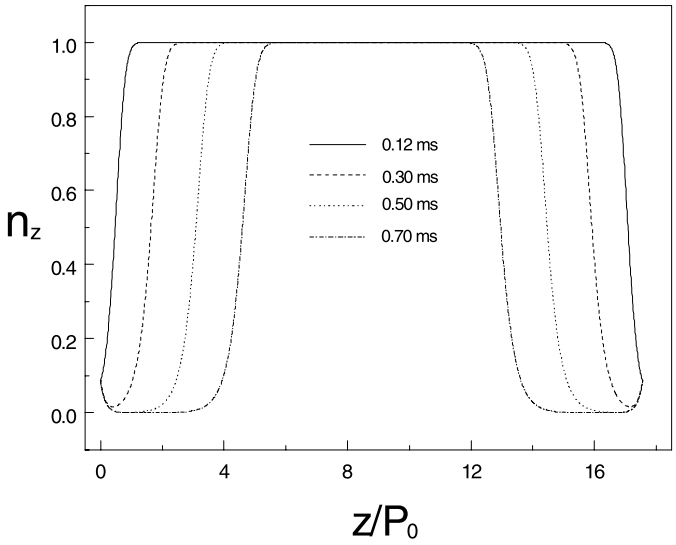

FIG. 7. Simulated time evolution of $n_z(z)$ during the initial H to P relaxation for the planar sample. The z axis is normal to the substrates.

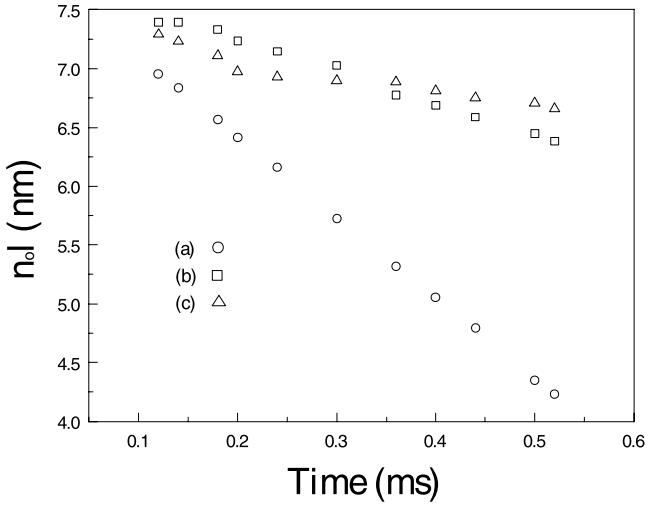

FIG. 8. Time variation of $n_o l$, the optical path length of the resonant cavity, calculated from (a) the simulated director configurations, (b) the simulated reflection spectra, and (c) the experimental reflection spectra.

In the figure the wavelength of peak reflectance λ_c decreases after 0.5 ms, and then evolves to the value of the equilibrium P state. This suggests that the TP state has been lasting for about 0.5 ms, and then a transition to the FC state takes place before the system reaches a complete twisted structure of the perfect TP state [7,8]. The relatively small reflection intensity of the TP state compared with that of the equilibrium P state also supports the presumption that a transition to the FC state has occurred before the perfect helical structure is formed throughout the cell.

Figure 7 shows the simulated time evolution of the z component of the director (n_z) during the early stages of the H to P transition. The region where $n_z \approx 1$ has a nematic structure and the region where $n_z \approx 0$ has a helical structure. As can be seen in the figure the nematic layer is reduced as time goes on. This means that the length of cavity resonator of the Fabry-Perot interferometric structure is reduced and, as a result, the wavelength intervals between the interference peaks increase. The cavity length calculated from the simulation and also from the experimental reflection spectra show this reduction with time very well. Figure 8 shows the change of the cavity length multiplied by the ordinary refractive index of the liquid crystal $n_o l$, i.e., the optical path length of the cavity, calculated from (a) the simulated director configurations, (b) the simulated reflection spectra, and (c) the experimental reflection spectra during the evolution of the TP state. All three graphs display a nearly linear decrement of $n_o l$ with time. However, the case (a) behaves differently with a much steeper reduction rate than the other two cases, between which quite a good agreement is observed. This reduction of $n_o l$ with time means that the physical length of the cavity, i.e., the nematic region of the material, reduces and the cholesteric phase expands toward the center of the cell. The fact that the cavity lengths calculated from both the experimental and simulated reflection spectra are longer than the values calculated from the director configurations seems to indicate that unlike the light reflections occurring at the mirrors of the conventional Fabry-Perot interferometer, the incident light into the cell is reflected from the periodically arrayed cholesteric helices rather than at the boundaries between the nematic and cholesteric phase. Therefore, the effective length of the cavity resonator that the light experiences is longer than the length of the nematic layer.

IV. CONCLUSION

We studied the growth and propagation process of the TP state during the H to P transition of a cholesteric liquid crystal system for planar boundary conditions. In the experimentally measured reflection spectra during the initial H-P relaxation, interference fringes are observed, the envelope of which corresponds to the broad reflection band of the TP state. This interference pattern is assumed to be caused by a Fabry-Perot interferometric structure, i.e., the spatially cholesteric-nematic-cholesteric structure formed in the cell. The numerically simulated reflection spectra obtained using the parameters for our sample also exhibits this Fabry-Perot-type interference fringes. The change in the fringe intervals with time obtained from the experimental and simulated reflection spectra also show that the length of the nematic layer reduces linearly with time as the material relaxes to the TP texture. These interference fringes observed in the reflection spectra and the reduction of the nematic layer with time are the experimental evidences that the TP state in a cholesteric material grows from the surfaces and propagates to the bulk for planar boundary conditions.

[1] P.G. de Gennes, Solid State Commun. **6**, 163 (1968).
[2] T. Ohtsuka, M. Tsukamoto, and M. Tsuchiya, Jpn. J. Appl. Phys. **12**, 371 (1973).
[3] M. Kawachi, O. Kogure, S. Yoshii, and Y. Kato, Jpn. J. Appl. Phys. **14**, 1063 (1975).
[4] D.-K. Yang and Z.-J. Lu, SID 95 Dig. Tech. Pap.-IEEE Int. Solid-State Circuits Conf. **26**, 351 (1995).
[5] P. Watson, J.E. Anderson, V. Seragan, and P.J. Bos, Liq. Cryst. **26**, 1307 (1999).
[6] Y.-C. Yang, M.-H. Lee, J.-E. Kim, H.Y. Park, and J.-C. Lee, Jpn. J. Appl. Phys. **40**, 649 (2001).
[7] P. Watson, V. Sergan, J.E. Anderson, and P.J. Bos, Liq. Cryst. **26**, 731 (1999).
[8] J.E. Anderson, P. Watson, T. Ernst, and P.J. Bos, Phys. Rev. E **61**, 3951 (2000).
[9] H. Mori, E.C. Gartland, Jr., J.R. Kelly, and P.J. Bos, Jpn. J. Appl. Phys. **38**, 135 (1999).
[10] H.A. van Sprang, Mol. Cryst. Liq. Cryst. **199**, 19 (1991).
[11] F. Grandjean, C. R. Acad. Soci., Paris **172**, 71 (1921).
[12] R. Cano, Bull. Soc. Fr. Mineral. Cristallogr. **90**, 333 (1967).
[13] P.G. de Gennes and J. Prost, *The Physics of Liquid Crystals* (Oxford University Press, New York, 1993).
[14] D.W. Berreman, Appl. Phys. Lett. **25**, 5 (1974).
[15] X.-D. Mi and D.-K. Yang, Dig. Tech. Pap.-IEEE Int. Solid-State Circuits Conf. **29**, 909 (1998).
[16] A. Rapini and M. Popoular, J. Phys. (Paris), Colloq. **30**, 54 (1969).
[17] D.W. Berreman, J. Opt. Soc. Am. **63**, 1374 (1973).
[18] W.L. Brogan, *Modern Control Theory*, 2nd ed. (Prentice-Hall, Englewood Cliffs, NJ, 1985).
[19] W.D. St. John, Z.-J. Lu, and J.W. Doane, J. Appl. Phys. **78**, 5253 (1995).
[20] M. Xu, F.-D. Xu, and D.-K. Yang, J. Appl. Phys. **83**, 1938 (1998).